3D structure of amyloid protofilaments of β_2-microglobulin fragment probed by solid-state NMR

Kentaro Iwata*, Toshimichi Fujiwara*, Yoh Matsuki*, Hideo Akutsu*, Satoshi Takahashi*, Hironobu Naiki†, and Yuji Goto*‡

*Institute for Protein Research, Osaka University and Core Research for Evolutional Science and Technology, Japan Science and Technology Agency, Suita, Osaka 565-0871, Japan; and †Faculty of Medical Sciences, University of Fukui and Core Research for Evolutional Science and Technology, Japan Science and Technology Agency, Matsuoka, Fukui 910-1193, Japan

Edited by Alan R. Fersht, University of Cambridge, Cambridge, United Kingdom, and approved October 4, 2006 (received for review August 18, 2006)

Understanding the structure and formation of amyloid fibrils, the filamentous aggregates of proteins and peptides, is crucial in preventing diseases caused by their deposition and, moreover, for obtaining further insight into the mechanism of protein folding and misfolding. We have combined solid-state NMR, x-ray fiber diffraction, and atomic force microscopy to reveal the 3D structure of amyloid protofilament-like fibrils formed by a 22-residue K3 peptide (Ser^{20}-Lys^{41}) of β_2-microglobulin, a protein responsible for dialysis-related amyloidosis. Although a uniformly ^{13}C,^{15}N-labeled sample was used for the NMR measurements, we could obtain the 3D structure of the fibrils on the basis of a large number of structural constraints. The conformation of K3 fibrils was found to be a β-strand–loop–β-strand with each K3 molecule stacked in a parallel and staggered manner. It is suggested that the fibrillar conformation is stabilized by intermolecular interactions, rather than by intramolecular hydrophobic packing as seen in globular proteins. Together with thermodynamic studies of the full-length protein, formation of the fibrils is likely to require side chains on the intermolecular surface to pack tightly against those of adjacent monomers. By revealing the structure of β_2-microglobulin protofilament-like fibrils, this work represents technical progress in analyzing amyloid fibrils in general through solid-state NMR.

2,2,2-trifluoroethanol | amyloid fibril | dialysis-related amyloidosis | protein misfolding | x-ray fiber diffraction

Amyloid fibrils are highly ordered filamentous aggregates formed by the self-assembly of peptides or proteins (1–4). There are currently ≈20 known diseases associated with deposition of amyloid fibrils, including Alzheimer's disease, type II diabetes, Parkinson's disease, and dialysis-related amyloidosis. Additionally, numerous peptides and proteins not directly related to diseases also can form amyloid-like fibrils *in vitro*, suggesting that amyloid fibril formation is a generic property of the polypeptide chain (2). To obtain further insight into protein folding and misfolding, it is crucial to clarify the mechanism of fibril formation and the structural stability of amyloid fibrils. Recently, it has been found that amyloid fibrils are, in general, amenable to the most sophisticated magic-angle-spinning (MAS) solid-state NMR methods, providing atomic-level structural information that otherwise has been inaccessible (5–10). These techniques, although focused on monomeric structural properties, shed light on a number of structural details and properties of fibril formation. Most recently, the structural details of whole fibrils have been proposed for amyloid-β fibrils (11). Combining various techniques, including solid-state NMR, closely related structural models for amyloid-β fibrils have been constructed (12, 13).

β_2-Microglobulin (β2-m), a component of the type I major histocompatibility antigen, forms amyloid fibrils in patients receiving hemodialysis for long periods (14, 15). Because of its clinical importance and suitable size for examining the relation between protein folding and amyloid formation, β2-m has been a target of extensive study on the relation between protein folding and amyloid fibril formation (14–18). In previous work, we found that a 22-residue K3 peptide (Ser^{20}-Lys^{41}), obtained by digesting β2-m, spontaneously forms amyloid protofilament-like fibrils *in vitro* (19). The K3 peptide is, therefore, an important system for detailed investigation of the structure and formation of amyloid fibrils.

K3 peptide forms fibrils over a wide range of pH and solvent conditions, both with and without the presence of alcohols (19–23). In particular, in 20% (vol/vol) 2,2,2-trifluoroethanol (TFE) and 10 mM HCl, long and thin fibrillar structures with a homogeneous thickness are formed (21–23). We consider these to be protofilaments, the individual filaments making up the mature amyloid fibrils. Here, we have used solid-state NMR, together with x-ray fiber diffraction and atomic force microscopy (AFM) measurements, to probe the structure of K3 fibrils. Because the K3 fibrils in 20% (vol/vol) TFE do not have a superstructure where several protofilaments associate with one another laterally (3), they are a suitable target for analyzing the whole fibril structure, excluding the contribution of the interfibril interactions. Even with a uniformly ^{13}C,^{15}N-labeled sample, we could propose the 3D structure of the fibrils, leading to an atomic-level understanding the protofibril structure and the types of interactions required to stabilize this structure.

Results

Fibril Morphology and X-Ray Fiber Diffraction. The K3 peptide forms two types of fibrillar structures with distinct morphology and secondary structure: "f210 fibrils" and "f218 fibrils," differing in the location of the minimum of the far-UV circular dichroism (CD) spectrum (23). The AFM images revealed a thin and long morphology (Fig. 1*A*), and the CD showed a strong negative ellipticity at 210 nm (Fig. 6, which is published as supporting information on the PNAS web site), confirming that the fibrils prepared in the present article correspond to the f210 fibrils (23). The thickness of the fibrils was homogeneous without a helical twist; fibril diameter ranged from 1.0 to 2.1 nm with a statistical average of 1.5 nm (±0.3). The x-ray fiber diffraction

Author contributions: K.I., H.N., and Y.G. designed research; K.I., T.F., Y.M., and S.T. performed research; H.A. and S.T. contributed new reagents/analytic tools; K.I., T.F., Y.M., and H.A. analyzed data; and K.I., T.F., and Y.G. wrote the paper.

The authors declare no conflict of interest.

This article is a PNAS direct submission.

Abbreviations: MAS, magic angle spinning; β2-m, β_2-microglobulin; TFE, 2,2,2-trifluoroethanol; AFM, atomic force microscopy; RFDR, rf-driven recoupling; DARR, dipolar-assisted rotational resonance.

Data deposition: The NMR chemical shifts have been deposited in the BioMagResBank, www.bmrb.wisc.edu (accession no. 10022).

‡To whom correspondence should be addressed. E-mail: ygoto@protein.osaka-u.ac.jp.

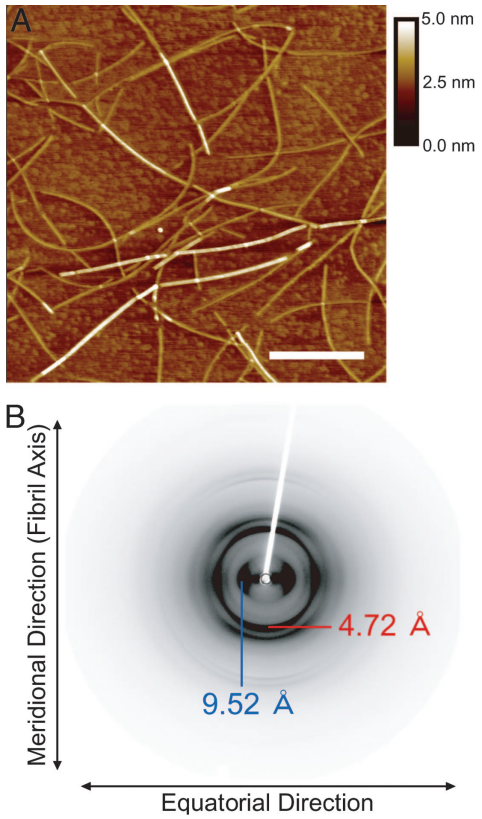

Fig. 1. AFM images and x-ray fiber diffraction of K3 fibrils. (*A*) AFM images of K3 fibrils formed in 20% (vol/vol) TFE/10 mM HCl. The scan was performed with a 25-fold diluted sample on a freshly cleaved mica surface. The white scale bar represents 500 nm, and the scan size is 2.5 × 2.5 μm with 512 × 512 points. (*B*) X-ray fiber diffraction of the K3 fibrils with incident beam perpendicular to the fibril axis. The data shows a typical cross-β pattern. The diffractions corresponding to 4.72 Å (red) and 9.52 Å (blue) indicate the distance between β-strands in the β-sheet and β-sheet layers in the laminated structure, respectively.

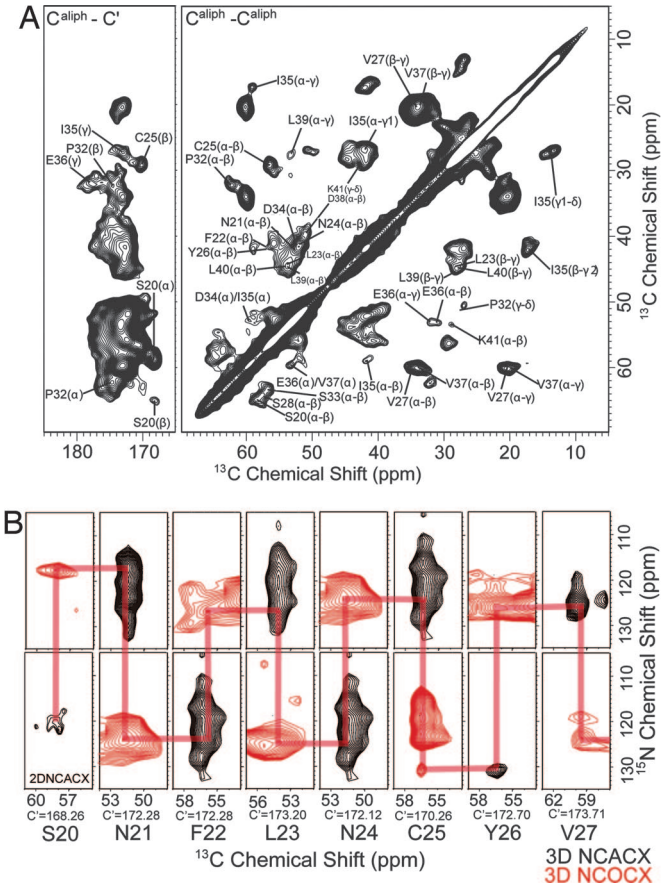

Fig. 2. ^{13}C–^{13}C and ^{15}N–^{13}C correlation NMR spectra of K3 fibrils. (*A*) 2D broadband ^{13}C–^{13}C correlation spectra for intraresidue correlations. The figure shows the expansion of the cross-peak regions for aliphatic-carbonyl carbons and aliphatic-aliphatic carbons. This spectrum was obtained at 16.4 T, with a MAS frequency of 16.0 kHz and a 4.00-ms mixing period during which an RFDR pulse sequence was applied. (*B*) 2D slices of the 3D ^{15}N–^{13}C intraresidue (NCACX) and sequential (NCOCX) correlation spectra. Black and red spectra indicate intraresidue and interresidue correlations, respectively. These spectra were obtained at 11.8 T and a MAS frequency of 12.5 kHz with 1.25-ms and 2.00-ms mixing periods during which the RFDR pulse sequence was applied for NCACX and NCOCX, respectively. Red lines indicate the sequential assignments.

showed a typical cross-β pattern (Fig. 1*B*). Strong bands with a characteristic spacing of 4.5–4.7 Å, typically observed for amyloid fibrils, were assigned to the distance between adjacent peptide chains in the β-sheets that comprise a cross-β structure. Other strong bands corresponding to a characteristic spacing of 9.4–9.8 Å represented the distance between the laminated β-sheets where peptide side chains are packed (24). Although several additional peaks were observed, they are difficult to assign because of their low quality (Fig. 7, which is published as supporting information on the PNAS web site).

Signal Assignments. To assign sequential resonances of K3 fibrils, we made a set of 2D and 3D ^{15}N–^{13}C and ^{13}C–^{13}C correlation experiments. Fig. 2*A* shows a 2D ^{13}C–^{13}C correlation spectrum obtained for fully labeled K3 fibrils with an rf-driven recoupling (RFDR) sequence at 4.0-ms mixing time. Cys, Gly, His, Pro, Ile, Glu, and Lys each appear once in K3. Pro^{32}, Ile^{35}, and Glu^{36} resonances were easily characterized with their characteristic chemical-shift pattern. In addition, sequential correlations were observed in the spectrum at 4.0-ms mixing time. Intramolecular peaks were distinguished from intermolecular peaks by comparing the spectra of the fully labeled sample with that of the spin-diluted sample in which a fraction of the labeled peptide was 1/3 (see below). These peaks enabled the assignment of overlapped peaks (Asn^{21}, Phe^{22}, Asp^{34}, and Val^{37}). Ser residues were well separated but could not be distinguished without sequential correlation data. Gly^{29} gave only the C′–C$^{\alpha}$ resonance overlapped with the C′–C$^{\beta}$ resonance of Leu residues. To distinguish multiple bond correlations, we also performed a 2D ^{13}C–^{13}C supercycled POST-C^{z} (SPC^{z}) 5 double-quantum experiment at a mixing time of 1.5 ms, yielding a spectrum that distinguishes one- and two-step dipolar correlations (Fig. 8, which is published as supporting information on the PNAS web site). The spectrum clearly indicated the C′–C$^{\alpha}$ peak of Gly^{29}.

To assign the side-chain resonances, we also performed a double-quantum/single-quantum correlation experiment (INADEQUATE; Fig. 9, which is published as supporting information on the PNAS web site). However, because of small chemical-shift differences in some residues, their peaks were overlapped. To separate signal sets in an additional dimension, 3D ^{15}N–^{13}C correlation experiments were conducted by using SPECIFIC CP transfers and RFDR ^{13}C–^{13}C mixing blocks (Fig. 2*B*). Analysis of a series of ^{13}C–^{13}C (Fig. 10, which is published as supporting information on the PNAS web site) and ^{15}N–^{13}C 2D and 3D spectra led to the main-chain signal assignments of all residues. For some residues, we confirmed the chemical shift by ^{13}C–^{13}C spin-diffusion experiments with dipolar-assisted rotational res-

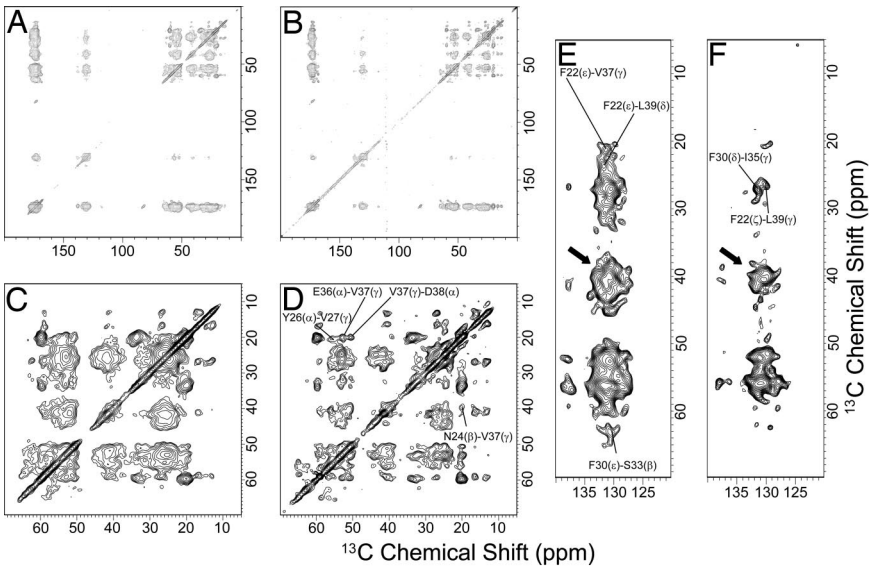

Fig. 3. 2D ^{13}C–^{13}C spin-diffusion experiments (DARR) with the fully labeled fibrils and spin-diluted fibrils. These spectra were recorded at 16.4 T with a 350-ms mixing period for the spin-diffusion experiment at a 16.0–kHz MAS frequency. (*A*, *C*, and *E*) The ^{13}C–^{13}C correlation spectrum obtained with the fully labeled fibrils. (*B*, *D*, and *F*) The ^{13}C–^{13}C correlation spectrum obtained with the spin-diluted fibrils. (*C* and *D*) Expansions of aliphatic regions. (*E* and *F*) Expansions of the cross-peak regions between aliphatic and aromatic carbons. The arrows indicate the regions of MAS side bands of aromatic carbon signals.

onance (DARR) at short mixing times (<20 ms). The summary of obtained chemical shifts is shown in Table 2, which is published as supporting information on the PNAS web site.

Constraints Based on the Chemical Shifts. The N, C^{α}, C^{β}, and C′ chemical shifts were analyzed with the program TALOS, which predicts dihedral angles from secondary chemical shifts (25). For Asn^{21}-Ser^{28} and Ser^{33}-Leu^{40}, satisfactory convergence was obtained, enabling the φ and ψ values to be predicted. These predicted angles were in the β-strand region of the Ramachandran plot. Moreover, the conformation of the peptide bond between His^{31} and Pro^{32} could be determined from the chemical-shift data. The difference of 5.3 ppm between the $^{13}C^{\beta}$ and $^{13}C^{\gamma}$ chemical shifts for Pro^{32} in K3 fibrils indicates that the His^{31}-Pro^{32} peptide bond assumes a trans conformation (26). Although this isomer is common in peptides and globular proteins, the native β2-m has a cis conformation at the His^{31}-Pro^{32} peptide bond, which plays an important role in the slow refolding of β2-m (27).

Tertiary Contacts in the K3 fibrils. To reveal the tertiary structure of the K3 fibrils, a series of ^{13}C–^{13}C spin-diffusion experiments with DARR were applied to both the fully labeled and spin-diluted samples. Various spin-diffusion spectra of K3 fibrils were obtained with mixing times ranging between 2.5 ms and 500 ms. Fig. 3 *A–D* shows spectra of both the fully labeled and the spin-diluted fibrils at a mixing time of 350 ms. Comparison of the spectra revealed that each monomer makes contact with adjacent monomers at many sites. Although many overlapping peaks were observed in the spectra of fully labeled samples, the spectra of spin-diluted samples, which were dominated by intramolecular correlations, were relatively well separated. Most strong cross-peaks corresponded to intraresidue correlations, but some peaks corresponded to long-range contacts. In particular, we observed cross-peaks that can be assigned to the F22ζ-L39γ, F30δ-I35γ, and N24β-V37γ correlations. These peaks represent intramolecular packing, indicating that K3 has a bend ranging from Gly^{29} to Pro^{32} (Fig. 3). These cross-peaks were observed at the mixing time of 350 ms as reported for the interresidue contact in β-amyloid (11). On the other hand, several intermolecular cross-peaks also were identified by comparing the peak intensities of fully labeled fibrils with those of spin-diluted fibrils (Fig. 11, which is published as supporting information on the PNAS web site). The spectra at a mixing time of 350 ms showed the contact of the Phe^{22} side chain with Leu^{39} C^{δ} of an adjacent K3 monomer. The contact of the Phe^{22} side chain with Val^{37} C^{γ} also was indicated by the spin-diffusion spectra at 350 ms.

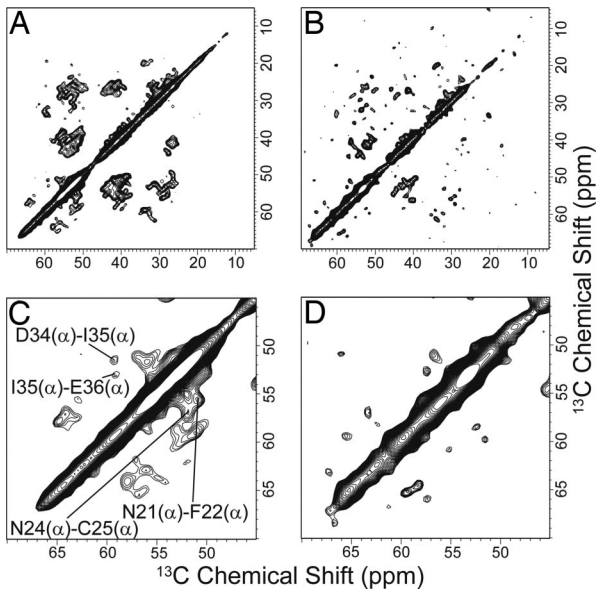

Fig. 4. 2D ^{13}C–^{13}C correlation spectra obtained with ^{1}H–^{1}H spin-diffusion (CHHC) experiments. (*A*) The spectrum obtained with fully labeled fibrils. The correlation between C^{α}–C^{α} carbons is indicated. (*B*) The spectrum obtained with spin-diluted fibrils. (*C*) Expansion of the C^{α} carbon region in the spectrum of fully labeled fibrils. (*D*) Expansion of the C^{α} carbon regions in the spectrum o f spin-diluted fibrils. Note that the C^{α}–C^{α} cross-peaks are significantly reduced. This reduction indicates that the cross-peaks contain intermolecular correlations. These spectra were obtained at 14.1 T with a 210-μs mixing period for the ^{1}H–^{1}H spin-diffusion experiment at a MAS frequency of 14.0 kHz.

BIOPHYSICS

Table 1. Summary of restraints for K3 amyloid fibrils

Restraints	Value
Total experimental restraints	61
Total distance restraints	27
Total ^{13}C–^{13}C restraints	27
Intramolecular restraints	13
Intermolecular restraints	14
Restraints in the class 2.0–3.5 Å	2
Restraints in the class 3.5–4.5 Å	15
Restraints in the class 4.5–6.5 Å	10
Total backbone dihedral angle restraints	34
Chemical shift-based restraints (TALOS)	34
Energies kcal/mol	
Final energies	106.0
Energies of bonds	3.3
Energies of angles	65.6
Energies of impropers	2.5
Energies of van der Waals	31.8
rms deviation	
Bonds, Å^2	0.02
Angles, °	0.42
Impropers, °	0.15
Backbone of the tetramer	1.67
Backbone of the middle monomer	1.43

The ^{13}C–^{13}C restraints were obtained with 2D spin-diffusion experiments. The energy and rms deviations are averaged value of the 10 lowest-energy structures among 50 calculated structures.

^{1}H-^{1}H Spin-Diffusion (CHHC) Experiments. To determine the sheet topology and the registry of hydrogen bonds in the fibrils, we carried out ^{1}H–^{1}H spin-diffusion experiments. With a ^{1}H mixing time of ≈250 μs, antiparallel β-sheets give strong single-bond C^α-C^α cross-peaks, whereas parallel β-sheets give much weaker peaks (28, 29) (Fig. 12, which is published as supporting information on the PNAS web site). Fig. 4 *A* and *B* shows the 2D correlation spectra obtained from the ^{1}H–^{1}H spin-diffusion experiment at a ^{1}H mixing time of 210 μs for the fully labeled and spin-diluted fibrils, respectively. In the spin-diluted fibrils, the ratio of the labeled and unlabeled samples was 1:2. Some interresidue C^α–C^α peaks between residues *i* and *i* + 1, which were much weaker than one-bond correlation peaks, were observed in the spectra of fully labeled fibrils, whereas these were strikingly reduced in the same experiment for the spin-diluted fibrils. The C^α–C^α peaks reflect the correlation between residues *i* and residues *i* + 1 of adjacent K3 molecules as well as sequential correlations. The result is consistent only with a parallel β-sheet geometry in which each residue in the fibril is in-register and each monomer is in nearly the same local conformation.

Calculation of the 3D Structure. The 34 dihedral angle restraints from the TALOS prediction, along with distance constraints from the other NMR measurements, yield a total of 55 restraints (Table 1). Among the 27 ^{13}C distance restraints from the spin-diffusion experiments, there are 13 and 14 interresidue and intermolecular restraints, respectively. In the present study, we can exclude the contacts between protofilaments, because the K3 fibrils consist of only one protofilament (see *Discussion*). Although we can distinguish intra- and intermolecular correlations for the two β-strands in a molecule, the obtained correlations are not sufficient to specify an interacting molecule in a group of molecules in the vicinity. This insufficiency allows the possibility of the strand assemblies with different degrees and directions of stagger (11, 12). Here, we assumed the structures in STAG(+1) and STAG(−1) following the definition of Petkova *et al*. (11). When the N- and C-terminal β-strands of each K3 molecule are located back and front, respectively, the C-terminal β-strand in the STAG(+1) model is displaced upward by a half of the interstrand distance (i.e., 4.7 Å) (see figure 7 of ref. 11). On the other hand, in the STAG(−1) model, the C-terminal β-strand is displaced downward by a half of the interstrand distance. Additionally, intermolecular restraints attributable to hydrogen bonds were added in β-strand regions predicted by TALOS. The restraints were arranged such that each residue in the fibril paired in-register in a parallel β-sheet orientation.

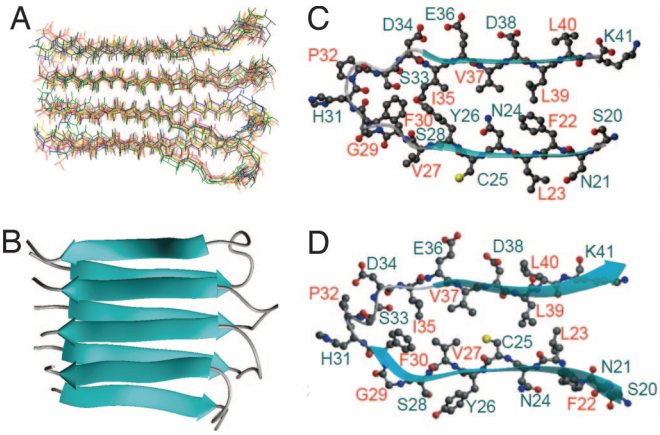

Fig. 5. 3D structures of tetrameric K3 and monomeric K3 in the fibrillar state. The conformation of K3 in the fibrillar state obtained by simulated annealing molecular dynamics by using CNS. (*A*) Calculated ensemble of tetrameric structures of K3 fibrils. (*B*) Ribbon model representation of tetrameric K3 in parallel STAG(+1) conformation. (*C*) The conformation of one K3 structure in the fibrillar state. (*D*) Comparison of the conformation of the K3 region in the crystal structure of native β2-m. Notably, the residues between Phe^{22} and Ser^{28} are flipped relative to the crystal structure of native β2-m in the fibrillar state.

The tetrameric structure of the K3 fibril was calculated by using the above restraints in a simulated annealing molecular dynamics structure optimization with the program CNS. Fig. 5*A* shows 10 lowest energy structures among 50 calculated structures. The calculation showed that only the STAG(+1) model, as is obvious in Fig. 5*B*, is consistent with our experimental restraints; probably, trans isomerism of Pro^{32} is important for assuming this staggered conformation. The main-chain root mean square deviation for these 10 structures was 1.68 Å for the K3 tetramers and 1.43 Å for the two K3 molecules located in the interior. The high degree of divergence of these structures was not attributable to the flexibility of fibrils but to the lack of long range structural constraints. The overall 3D structure of K3 in the fibrillar state is β(Asn^{21}-Ser^{28})–loop(Gly^{29}-Pro^{32})–β(Ser^{33}-Lys^{40}) in a parallel β-sheet assembly in the STAG(+1) mode. Importantly, the calculated structure is different from the native structure in that nonpolar residues (Val^{27}, Cys^{25}, and Leu^{23}) buried in the interior of the Ig fold are exposed to the surface (see *Discussion*).

Mutational Analysis of Phe Residues. Aromatic amino acids have been suggested to be important for amyloid fibril formation (30). The aromatic residues of K3 are Phe^{22}, Tyr^{26}, and Phe^{30}. Assuming a β-strand–loop–β-strand conformation with a parallel β-sheet topology, π–π interactions between the same aromatic residues of adjacent peptides might be important for fibril formation. To investigate the role of Phe side chains in K3 fibril formation, two mutants with Phe^{22}-Ala or Phe^{30}-Ala substitutions were synthesized. Although wild-type K3 formed fibrils spontaneously in 20% (vol/vol) TFE and 10 mM HCl with a large negative intensity at 210 nm (i.e., f210 fibrils), the CD

spectrum (Fig. 6) indicates that these mutants did not form fibrils. These results might be attributable to an increased barrier of fibril nucleation. Thus, seed-dependent fibrillization assays of K3 mutants also were performed by using wild-type K3 seeds. However, no notable fibrillation was observed, indicating that the removal of Phe^{22} or Phe^{30} strikingly inhibits the fibril formation.

Discussion

K3 Fibrils Consist of Two-Layered, Parallel, and Staggered β-Sheets. The goal of the present study was to determine the 3D structure of K3 fibrils formed in 20% (vol/vol) TFE and 10 mM HCl. Mature amyloid fibrils consist of several β-sheets stabilized by hydrophobic interactions (4, 10). In analogy with the structural hierarchy of globular proteins, Petkova *et al*. (11) defined primary, secondary, tertiary, and quaternary structures of amyloid fibrils. Although primary structure is defined similarly in globular proteins and amyloid fibrils, secondary structure in amyloid fibrils is mostly β-sheet, and the determination of secondary structure corresponds to the identification of the location of β-sheet regions. Tertiary structure in amyloid fibrils involves the parallel or antiparallel β-sheet orientation, and quaternary structure relates to the position and orientation of β-sheets relative to one another.

Thus, to construct the 3D structure of K3 fibrils, it is necessary to identify the number of β-sheet layers constituting the fibrils (i.e., quaternary structure). The x-ray fiber diffraction data indicated that the distances between adjacent peptide chains in the β-sheet and the laminated β-sheets are 4.5–4.7 Å and 9.5–10.0 Å, respectively, implying that the K3 fibrils consist of the least two β-sheet layers. If the fibrils have three layers of β-sheets, the fibril diameter would be >20 Å. Considering that the average diameter of K3 fibrils was ≈15 Å in AFM measurements, only a structure made of two layers of β-sheets is consistent. Most likely, the 5-Å difference between AFM measurements and the diffraction originates from the volume of exposed side chains: the distance between β-sheets is defined in terms of the backbone–backbone distance and does not include side chains. We conclude that the K3 fibril is made of two β-sheet layers, where each K3 molecule consists of two β-strands and a connecting loop. This minimal quaternary structure is an ideal system for analyzing the atomic structure and stabilization of amyloid fibrils.

The tertiary structure (i.e., orientation of β-sheets) also is required for complete structural determination. Solid-state ^{1}H–^{1}H spin-diffusion experiments revealed that K3 fibrils consist of parallel β-sheets with intermolecular hydrogen bonds formed between the same residues. To date, many proposed amyloid fibril models consist of parallel β-sheets (6, 11–13, 31), suggesting that the parallel orientation is preferred over the antiparallel orientation. However, it also has been reported that both parallel and antiparallel β-sheets exist even for fibrils formed from the same peptides (8, 32), suggesting that the orientation preference depends on the experimental conditions. The secondary structure of K3 fibrils as determined by TALOS was found to be β(Asn^{21}-Ser^{28})–loop(Gly^{29}-Pro^{32})–β(Ser^{33}-Lys^{40}). The distribution of secondary structures is basically consistent with reports of various fragments corresponding to the K3 region analyzed by vibrational spectroscopy (33, 34).

The 3D structure of the K3 tetramer was calculated by using the above hierarchical restraints, revealing that K3 in the fibrillar state assumes a β-strand–loop–β-strand conformation with each K3 molecule stacked in a parallel orientation with the STAG(+1) mode. The location of secondary structures are similar to those of the native structure: β(Ser^{20}-Phe^{30})–loop(His^{31}-I35)–β(Glu^{36}-Lys^{41}). To our surprise, the calculated structure was different from the native structure in that nonpolar residues (Val^{27}, Cys^{25}, and Leu^{23}) buried in the interior of the Ig fold are exposed to the surface. In the fibril form, aromatic Phe^{22} and Tyr^{26} and polar Gln^{24} and Ser^{28} are buried between the β-strands. Nevertheless, this structure is consistent with our previous UV absorption study, which indicated Tyr^{26} was buried in the interior of the fibrils (23). Additionally, the structure with exposed hydrophobic residues (Leu^{40}, Val^{27}, and Leu^{23}) is consistent with the report that the K3 fibrils prepared in 20% (vol/vol) TFE assemble laterally into mature fibrils after being transferred to a solution without TFE (22). The exposed hydrophobic side chains clearly play an important role in assembling protofibrils to form the mature fibrils.

Protofilaments Stabilized by Intermolecular Interactions. The validity of the calculated structure was examined by mutagenesis of K3 fragment. There are several reports on the role of side chains in the stabilization of amyloid structures (8, 11, 12, 30, 31, 35). We focused on the role of aromatic Phe side chains. In the calculated structure, the Phe rings are aligned and separated by a distance of 4.5–4.7 Å (i.e., the interstrand spacing), a distance favorable for π–π interactions (36). The mutational analysis showed that the Phe to Ala substitutions inhibited the amyloid fibril formation, even though Phe^{30} is located in a loop region in the calculated structure (Fig. 6*C*).

Moreover, the role of Tyr^{26} buried between the β-sheets is intriguing: it is conceivable that the Tyr^{26} residues also are stabilized by π–π interactions, although such interactions are not obvious from the calculated structure: the phenol ring of Tyr^{26} runs parallel to the plane of the β-sheets. Another side-chain interaction that has been described previously is the "Asn ladder" formed by Asn^{24} (31, 37). According to the calculated fibrillar structure, the side chain of Asn^{24} is located in the interior of the fibrils, namely, in a hydrophobic environment not thermodynamically favorable for the isolated polar amide group. To avoid this energetic disadvantage, the amide groups of aligned Asn^{24} residues are likely to form an intermolecular hydrogen-bond network with adjacent molecules.

These characteristics of the calculated structure and the results of mutagenesis indicate that the fibrillar structure assembles so as to optimize intermolecular interactions between neighboring K3 peptides rather than intramolecular packing, as seen in globular proteins. This consideration is supported by the conformational difference between the fibrillar and native β2-m structures (Fig. 5 *C* and *D*). The K3 peptide corresponds to β-strands B and C with the connecting B–C loop in the native β2-m. Although a similar β-strand–loop–β-strand geometry is observed in the fibrils, the residues between Phe^{22} and Ser^{28} are flipped relative to the fibrillar state. This marked difference in the interstrand interactions probably leads to a less tightly packed interior of K3 fibrils in comparison with that of the native structure.

Conclusions

Recent 2D and 3D solid-state NMR methods provide sufficient inter- and intraresidue correlations for nearly complete signal assignment of this 22-residue peptide in a noncrystalline state. The resulting chemical shifts yield important dihedral angle constraints. Distance information can be obtained by ^{13}C-NMR detection of ^{1}H-^{1}H and ^{13}C-^{13}C spin diffusion in a uniformly labeled fibril. The intra- and intermolecular distances can be distinguished by isotope dilution with natural-abundance molecules. Together, even with a uniformly ^{13}C,^{15}N-labeled sample, it was possible to construct the 3D structure of the fibrillar form of K3. The fibrillar state consisted of a β-strand–loop–β-strand conformation with the K3 molecules stacked in a parallel manner with the STAG(+1) mode, where maximization of the intermolecular interactions, in particular aromatic π–π interactions, is achieved rather than optimal intramolecular packing. The overall structure resembles the fibril structures of Aβ(1–40)

(11), Aβ(1–42) (12), and the HET-s fragment (6), suggesting that it is a common structural motif of amyloid protofibrils. Together with thermodynamic studies of full-length β2-m (38, 39), it is likely for side chains on the intermolecular surface to be tightly packed with adjacent monomers, otherwise loose packing with cavities would be observed.

Materials and Methods

K3 and Mutant Peptides. Recombinant human β2-m and ^{13}C,^{15}N-labeled β2-m was expressed in *Escherichia coli* and purified as described previously (27, 40). K3 peptide was obtained by digestion of β2-m with lysyl endopeptidase (*Achromobacter* protease I) as described in ref. 19. K3 and its mutant peptides also were synthesized by the Fmoc method in a step-wise fashion on 0.1 mmol of preloaded Fmoc-Ala-PEG-polystylene resin with a Pioneer peptide synthesizer (Applied Biosystems, Foster City, CA). Details are provided in *Supporting Materials and Methods*, which is published as supporting information on the PNAS web site.

Fibril formation of K3 was performed for one day at 25°C by using a final peptide concentration of 100 μM in 20% (vol/vol) TFE, 10 mM HCl, and 1 mM NaCl (23). For the spin-diluted fibrils for solid-state NMR, a mixture of the labeled and non-labeled K3 peptides at a molar ration of 1:2 was dissolved in 10 mM NaOH and polymerized in the same way.

AFM, X-Ray Fiber Diffraction, and CD Measurements. AFM images were obtained by using a dynamic force microscope (Nano Scope IIIa; Digital Instruments, Woodbury, NY). X-ray fiber diffraction of partly aligned K3 fibrils by centrifugation were collected at a SPring-8 (Hyogo, Japan), BL44XU beamline at room temperature. Far-UV CD spectra were measured with an AVIV model 215s spectropolarimeter (AVIV Association, Lakewood, NJ). Details are provided in *Supporting Materials and Methods*.

Solid-State NMR. The pellets obtained by centrifugation were dried into films with silica gel at 4°C for 5–7 days. The films were ground down and packed into a 3.2-mm NMR spinner. All of the experiments were performed with Varian/Chemagnetics (Palo Alto, CA) Infinity-500, Infinity-600, and Infinity-700 spectrometers operating at ^{13}C NMR frequencies of 125.6, 150.0, and 175.9 MHz, respectively. The experiments were performed with double (^{1}H,^{13}C)- and triple (^{1}H,^{13}C,^{15}N)-resonance T3 probes equipped with a 3.2-mm spinner module. The MAS frequencies were kept at 12.5, 14.0, and 16.0 kHz, respectively. The probe temperature was maintained at -20 to -30°C. Details are provided in *Supporting Materials and Methods*.

Structure Calculation. The structure of the fibrillar conformation of the K3 peptide was calculated by using CNS version 1.1 by applying the molecular dynamics simulated annealing protocol with torsion angles as internal degrees of freedom. Four K3 peptides were used in the simulation. The annealing protocol consisted of high-temperature sampling at 50,000 K for 1,000 steps with 8 ps per step and subsequent cooling to 0 K in 1,000 steps. Experimental carbon–carbon distance restrains, backbone dihedral angle restraints obtained by TALOS, and intermolecular constraints of hydrogen bonds for parallel β-sheet among the β-sheet regions were used for structure refinement. All structures have been energy-minimized, and the 10 lowest-energy structures among 50 calculated structures have been selected and further analyzed. Figures of the final structures were drawn with MOLMOL (41).

We thank Professor Atsushi Nakagawa and Dr. Takanori Matsuura for x-ray fiber diffraction data collection and Dr. Daron Standley for helpful discussions. This work was supported by Takeda Science Foundation and Grant-in-Aid for Priority Areas 40153770 from the Japanese Ministry of Education, Culture, Sports, Science, and Technology.

1. Kelly JW (1998) *Curr Opin Struct Biol* 8:101–106.
2. Dobson CM (2003) *Nature* 426:884–890.
3. Jiménez JL, Nettleton EJ, Bouchard M, Robinson CV, Dobson CM, Saibil HR (2002) *Proc Natl Acad Sci USA* 99:9196–9201.
4. Makin OS, Serpell LC (2005) *FEBS J* 272:5950–5961.
5. Jaroniec CP, MacPhee CE, Bajaj VS, McMahon MT, Dobson CM, Griffin RG (2004) *Proc Natl Acad Sci USA* 101:711–716.
6. Ritter C, Maddelein M, Siemer AB, Lührs T, Ernst M, Meier BH, Saupe SJ, Riek R (2005) *Nature* 435:844–848.
7. Heise H, Hoyer W, Becker S, Andronesi OC, Riedel D, Baldus M (2005) *Proc Natl Acad Sci USA* 102:15871–15876.
8. Naito A, Kamihira M, Inoue R, Saitô, H (2004) *Magn Reson Chem* 42:247–257.
9. Petkova AT, Ishii Y, Balbach JJ, Antzutkin ON, Leapman RD, Delaglio F, Tycko R (2002) *Proc Natl Acad Sci USA* 99:16742–16747.
10. Petkova AT, Leapman RD, Guo Z, Yau W, Mattson MP, Tycko R (2005) *Science* 307:262–265.
11. Petkova AT, Yau W, Tycko R (2006) *Biochemistry* 45:498–512.
12. Lührs T, Ritter C, Adrian M, Riek-Loher D, Bohrmann B, Döbeli H, Schubert D, Riek R (2005) *Proc Natl Acad Sci USA* 102:17342–17347.
13. Shivaprasad S, Wetzel R (2004) *Biochemistry* 43:15310–15317.
14. Naiki H, Hashimoto N, Suzuki S, Kimura H, Nakakuki K, Gejyo F (1997) *Amyloid* 4:223–232.
15. Jahn TR, Radford SE (2005) in *Amyloid Proteins. The Beta Sheet Conformation and Disease*, ed Sipe JD (Wiley, Weinheim), pp 667–695.
16. Hoshino M, Katou H, Hagihara Y, Hasegawa K, Naiki H, Goto Y (2002) *Nat Struct Biol* 9:332–336.
17. Katou H, Kanno T, Hoshino M, Hagihara Y, Tanaka H, Kawai T, Hasegawa K, Naiki H, Goto Y (2002) *Protein Sci* 11:2218–2229.
18. Jahn TR, Parker MJ, Homans SW, Radford SE (2006) *Nat Struct Mol Biol* 13:195–201.
19. Kozhukh GV, Hagihara Y, Kawakami T, Hasegawa K, Naiki H, Goto Y (2001) *J Biol Chem* 277:1310–1315.
20. Ohhashi Y, Hasegawa K, Naiki H, Goto Y (2004) *J Biol Chem* 279:10814–10821.
21. Wadai H, Yamaguchi K, Takahashi S, Kanno T, Kawai T, Naiki H, Goto Y (2005) *Biochemistry* 44:157–164.
22. Kanno T, Yamaguchi K, Naiki H, Goto Y, Kawai T (2005) *J Struct Biol* 149:213–218.
23. Yamaguchi K, Takahashi S, Kawai T, Naiki H, Goto Y (2005) *J Mol Biol* 352:952–960.
24. Fändrich M, Dobson CM (2002) *EMBO J* 21:5682–5690.
25. Cornilescu G, Delaglio F, Bax A (1999) *J Biomol NMR* 13:289–302.
26. Sarkar SK, Torchia DA, Kopple KD, VanderHart DL (1984) *J Am Chem Soc* 106:3328–3331.
27. Kameda A, Hoshino M, Higurashi T, Takahashi S, Naiki H, Goto Y (2005) *J Mol Biol* 348:383–397.
28. Tang M, Waring AJ, Hong M (2005) *J Am Chem Soc* 127:13919–13927.
29. Tycko R, Ishii Y (2003) *J Am Chem Soc* 125:13948–13956.
30. Gazit E (2002) *FASEB J* 16:77–83.
31. Nelson R, Sawaya MR, Balbirnie M, Madsen AO, Riekel C, Grothe R, Eisenberg D (2005) *Nature* 435:773–778.
32. Petkova AT, Buntkowsky G, Dyda F, Leapman RD, Yau WM, Tycko R (2004) *J Mol Biol* 335:247–260.
33. Hiramatsu H, Goto Y, Naiki H, Kitagawa T (2004) *J Am Chem Soc* 126:3008–3009.
34. Hiramatsu H, Goto Y, Naiki H, Kitagawa T (2005) *J Am Chem Soc* 127:7988–7989.
35. Perutz MF, Finch JT, Berriman J, Lesk A (2002) *Proc Natl Acad Sci USA* 99:5591–5595.
36. Chelli R, Gervasio FL, Procacci P, Schettino V (2002) *J Am Chem Soc* 124:6133–6143.
37. Kajava AV, Aebi U, Steven AC (2005) *J Mol Biol* 348:247–252.
38. Kardos J, Yamamoto K, Hasegawa K, Naiki H, Goto Y (2004) *J Biol Chem* 279:55308–55314.
39. Chatani E, Kato M, Kawai T, Naiki H, Goto Y (2005) *J Mol Biol* 352:941–951.
40. Chiba T, Hagihara Y, Higurashi T, Hasegawa K, Naiki H, Goto Y (2003) *J Biol Chem* 278:47016–47024.
41. Koradi R, Billeter M, Wüthrich K (1996) *J Mol Graphics* 14:51–55.